01 May 2015

Kinetic Isotope Effect of the $^{16}O+^{36}O_2$ and $^{18}O+^{32}O_2$ Isotope Exchange Reactions: Dominant Role of Reactive Resonances Revealed by an Accurate Time-Dependent Quantum Wavepacket Study

Zhigang Sun

Dequan Yu

Wenbo Xie

Jiayi Hou

et. al. For a complete list of authors, see https://scholarsmine.mst.edu/chem_facwork/2132

Recommended Citation

Z. Sun et al., "Kinetic Isotope Effect of the $^{16}O+^{36}O_2$ and $^{18}O+^{32}O_2$ Isotope Exchange Reactions: Dominant Role of Reactive Resonances Revealed by an Accurate Time-Dependent Quantum Wavepacket Study," *Journal of Chemical Physics*, vol. 142, no. 17, American Institute of Physics (AIP), May 2015.
The definitive version is available at https://doi.org/10.1063/1.4919861

Kinetic isotope effect of the $^{16}O + {}^{36}O_2$ and $^{18}O + {}^{32}O_2$ isotope exchange reactions: Dominant role of reactive resonances revealed by an accurate time-dependent quantum wavepacket study

Zhigang Sun,[1,a)] Dequan Yu,[1] Wenbo Xie,[1] Jiayi Hou,[1] Richard Dawes,[2] and Hua Guo[3]
[1]*State Key Laboratory of Molecular Reaction Dynamics and Center for Theoretical and Computational Chemistry, Dalian Institute of Chemical Physics, Chinese Academy of Sciences, Dalian 116023, China and Center for Advanced Chemical Physics and 2011 Frontier Center for Quantum Science and Technology, University of Science and Technology of China, 96 Jinzhai Road, Hefei 230026, China*
[2]*Department of Chemistry, Missouri University of Science and Technology, Rolla, Missouri 65409, USA*
[3]*Department of Chemistry and Chemical Biology, University of New Mexico, Albuquerque, New Mexico 87131, USA*

(Received 12 February 2015; accepted 27 April 2015; published online 7 May 2015)

The $O + O_2$ isotope exchange reactions play an important role in determining the oxygen isotopic composition of a number of trace gases in the atmosphere, and their temperature dependence and kinetic isotope effects (KIEs) provide important constraints on our understanding of the origin and mechanism of these and other unusual oxygen KIEs important in the atmosphere. This work reports a quantum dynamics study of the title reactions on the newly constructed Dawes-Lolur-Li-Jiang-Guo (DLLJG) potential energy surface (PES). The thermal reaction rate coefficients of both the $^{18}O + {}^{32}O_2$ and $^{16}O + {}^{36}O_2$ reactions obtained using the DLLJG PES exhibit a clear negative temperature dependence, in sharp contrast with the positive temperature dependence obtained using the earlier modified Siebert-Schinke-Bittererova (mSSB) PES. In addition, the calculated KIE shows an improved agreement with the experiment. These results strongly support the absence of the "reef" structure in the entrance/exit channels of the DLLJG PES, which is present in the mSSB PES. The quantum dynamics results on both PESs attribute the marked KIE to strong near-threshold reactive resonances, presumably stemming from the mass differences and/or zero point energy difference between the diatomic reactant and product. The accurate characterization of the reactivity for these near-thermoneutral reactions immediately above the reaction threshold is important for correct characterization of the thermal reaction rate coefficients. © *2015 AIP Publishing LLC.* [http://dx.doi.org/10.1063/1.4919861]

I. INTRODUCTION

The isotope exchange reaction

$$^{x}O + {}^{y}O\,{}^{z}O \xrightarrow{O_3^*} {}^{z}O + {}^{x}O{}^{y}O \text{ or } {}^{y}O + {}^{x}O\,{}^{z}O,$$

where x, y, and z denote the 16, 17, and 18 isotopes of the oxygen atom, represents an elementary step in ozone formation and thus may influence ozone's isotopic composition. Thermal rate coefficients of various isotopic exchange reactions have been measured experimentally, all of which exhibit negative temperature dependences,[1–4] suggesting a barrierless complex-forming mechanism. Interestingly, a significant kinetic isotope effect (KIE) has also been observed for these near-thermoneutral reactions:[4] The reaction rate coefficient of the $^{18}O + {}^{32}O_2$ (conventionally abbreviated as 8+66) reaction is about 1.27 times that of the $^{16}O + {}^{36}O_2$ (conventionally abbreviated as 6+88) reaction at room temperature. The origin of this unexpectedly large KIE is still not clearly elucidated, but might be related to the energy difference due to differing zero-point energies (ZPEs) between the diatomic reactant and product,[4] which is an order of magnitude smaller (only ± 23 cm^{-1}) than the thermal energy ($2k_bT = 440$ cm^{-1})! It is also not clear how the KIEs in the exchange reactions influence the well-known and surprising mass-independent fractionation (MIF) of oxygen isotopes in atmospheric ozone.[5–8] However, the apparent correlation with the ZPE of the diatomic O_2 molecule involved in the MIF points to a quantum mechanical origin for these puzzling phenomena under unscrambled conditions.[9–11]

Despite the well-established complex-forming mechanism, the exchange reactions are known to have a strong non-statistical character. Recent crossed molecular beam experiments have shown that the $^{18}O + {}^{32}O_2 \rightarrow {}^{16}O + {}^{34}O_2$ exchange reaction is dominated by a forward bias in the differential cross section at two collision energies.[12,13] As a result, statistical models are not sufficient to describe the reaction dynamics and the understanding of these KIEs can only be satisfactorily achieved by quantum dynamical models.[6] Interestingly, the KIEs in ozone formation have also been shown to require a dynamical correction to the statistical treatment.[14]

A key pre-requisite for quantum dynamical studies of these reactions is an accurate potential energy surface (PES). The earlier Siebert-Schinke-Bittererova[15,16] PES of $O_3(X^1A')$ modified by Babikov *et al.*,[17] denoted as mSSB, has been widely used in dynamical calculations.[16,18–22] However, the

a)Author to whom correspondence should be addressed. Electronic mail: zsun@dicp.ac.cn

mSSB PES is now known to be insufficiently accurate, particularly in the asymptotic region. Indeed, the calculated rate coefficients for the exchange reactions on the mSSB PES are about three times smaller than the measured values and show positive dependences on temperature.[22] It has been pointed out by Schinke and coworkers[22] that the error can be traced to a submerged barrier in the asymptotic region, commonly seen in almost all previous *ab initio* calculations.[23–25] This so-called "reef" structure becomes a bottleneck with large impact parameters, thus reducing the reactivity and causing a positive temperature dependence. This key feature of the PES has recently been shown to be an artifact in the *ab initio* treatment of the O_3 electronic structure in the asymptotic region. With a higher level of *ab initio* theory, the "reef" disappears,[26,27] and the calculated rate coefficients are found in much better agreement with experiment with a negative temperature dependence.[28,29] Further quantum dynamics calculations on the latest Dawes-Lolur-Li-Jiang-Guo (DLLJG) PES[27] coupled with an accurate long-range potential[30] yielded both integral and differential cross sections (ICSs and DCSs)[31] that are in good agreement with the recent molecular beam experiments.[12,13] These results provide strong supporting evidence for the accuracy of the DLLJG PES. In addition, recent spectroscopic studies provided further evidence against the "reef" structure in the asymptotic region.[32]

Due to the largest ZPE differences in the product and reactant diatoms of the endoergic 6+88 (R1) and exoergic 8+66 (R2) reactions,

$$^{16}O + {}^{36}O_2 \rightarrow {}^{16}O{}^{18}O + {}^{18}O, \quad \text{(R1)}$$

$$^{18}O + {}^{32}O_2 \rightarrow {}^{18}O{}^{16}O + {}^{16}O, \quad \text{(R2)}$$

among all of the isotope exchange reactions, they represent ideal candidates for studying the KIE[21,33] and for understanding how the small ZPE differences might lead to marked KIEs in the exchange reactions. We have reported preliminary results on the negative temperature dependence of the rate coefficients in our recent communication,[28] which include the thermal rate coefficient of the 8+66 (R2) reaction and the rate coefficients of the 6+88 (R1) and 6+66 reactions for the lowest rotational state of the O_2 reactant. However, the KIE has not yet been discussed using quantum reactive scattering theory on either the DLLJG or mSSB PES. In addition, the threshold reactivity of (R1) was not very accurately determined due to the limited grid range applied. These issues are addressed here. We note that the same quantities have been studied in the accompanying paper by Honvault *et al.*[34] but using a different quantum method. Furthermore, we also report here the thermal reaction rate coefficient on the mSSB PES to examine if it assumes a negative temperature dependence when thermally populated rotational states of the O_2 reactant are included.

In this work, the kinetics of these reactions are studied using an efficient time-dependent wave packet (WP) method, where a 4th order split operator was applied to propagate the initial WP using a time step as large as 120 a.u. and an L-shape grid method.[35–38] The ICSs are obtained using an exact Hamiltonian, thus possessing no dynamical approximation. In addition, all thermally populated reactant rotational states are included, some approximately, in the calculation of the thermal rate coefficients. The results reported in this work are used to answer two key questions. First, what is the influence of the "reef" structure on kinetics? Second, does the ZPE difference fully account for the isotope effects in (R1) and (R2)?

The remainder of the paper is organized as follows. In Sec. II, the theoretical and numerical details of the calculations are given. The results and discussion are presented in Sec. III. We conclude in Sec. IV.

II. THEORETICAL METHODS

The quantum scattering theory for atom-diatom reactions is well established[39] and as a result, only a brief outline is given here. However, in the current study, we did not calculate the state-to-state S-matrix elements,[37,40] as in our previous work.[31] Instead, only the total reaction probabilities were calculated using a flux formalism in the reactant Jacobi coordinates (R, r, θ)[41] and used to assemble the total reaction cross sections by summing over the partial waves. The propagation of the WP was carried out using a 4th order split-operator, which has been discussed in detail in Refs. 35 and 38. In the calculation of the total reaction probability for a specified J and j_0, all of the helicity quantum numbers below K_{cut} are included. When smaller than $K_{\max} = \max(J, j_0)$, K_{cut} is set as $\max(j_0, 10, 2J/3)$. Otherwise, K_{cut} is set as $K_{\max}$. Our numerical tests have shown that such a truncation of the helicity quantum number introduces negligible errors for the studied reactions.

In calculating the ICS for a particular initial rotational state, the total reaction probabilities for $J \leq 30$ were computed explicitly. For higher J values, the reaction probabilities were approximated from those explicitly computed at J = 30, 40, ..., 80, and 90 using the well-known J-shifting rule,[42] which approximates the reaction probabilities for J values that were not calculated explicitly by shifting the reaction probability by a suitable amount. The largest partial wave for calculating the reaction probabilities of all initial states is J = 90 and the energy spacing is taken as 0.000 02 eV for collision energies lower than 0.006 eV but taken as 0.001 eV for higher collision energies. In this way, the initial state-specified ICS up to collision energy 0.2 eV and the initial state-specified thermal rate coefficients can be accurately determined.

The initial state-specific reaction rate coefficient for the initial state (v_0, j_0) is calculated by thermally averaging the translational energy of the corresponding cross section as

$$k_{v_0 j_0}(T) = Q_{el}^{-1} \left(\frac{8 k_b T}{\pi \mu R} \right)^{1/2} (k_b T)^{-2} \int_0^\infty E e^{-E/k_b T} \sigma_{v_0 j_0}(E)\, dE, \quad (1)$$

where k_b is the Boltzmann's constant and T is the temperature in Kelvin. Q_{el} is the electronic partition function for the exchange reaction, which is given by[43]

$$Q_{el} = 3\left[5 + 3\exp(-227.6/T) + \exp(-325.9/T)\right]. \quad (2)$$

The thermal reaction rate coefficient can be calculated from the Boltzmann averaging of the initial state-specific reaction rate

coefficients as

$$k(T) = \frac{\sum_{v_0 j_0} (2j_0 + 1)\, k_{v_0 j_0}(T)\, e^{-E_{v_0 j_0}/k_b T}}{\sum_{v_0 j_0} (2j_0 + 1)\, e^{-E_{v_0 j_0}/k_b T}}, \quad (3)$$

where $E_{v_0 j_0}$ is the rovibrational energy of the diatomic molecule of the reagent.

Nuclear spin statistics restrict the $^{32}O_2$ and $^{36}O_2$ molecules to rotational states with odd quantum numbers. Hence, the initial state specified reaction rate coefficients for all initial rotational states of odd quantum numbers up to $j_0 = 29$ have been included. Vibrational excitation in the reactant is not considered as the corresponding Boltzmann weight is very small. It is very time-consuming for a complete calculation for all relevant initial rotational states. In practice, only ICSs for initial rotational states of quantum numbers $j_0 = 1$, 5, 9, and 21 were calculated using the time-dependent quantum WP method. The ICSs of other rotational states lower than $j_0 = 21$ were then calculated by a j_0-interpolation method as follows:

$$\sigma_{v_0, j_0}(E_c) = \frac{E_{j_0} - E_{j_0^s}}{E_{j_0^l} - E_{j_0^s}} \sigma_{v_0, j_0^l}(E_c) + \frac{E_{j_0^l} - E_{j_0}}{E_{j_0^l} - E_{j_0^s}} \sigma_{v_0, j_0^s}(E_c), \quad (4)$$

where j_0^l and j_0^s are the rotational quantum numbers larger (l) or smaller (s) than j_0^i, respectively. E_{j_0} is the energy of the rotational state j_0. This method was applied in our previous study,[28] and we test its validity here by comparing the ICS obtained by the wavepacket method and the j_0-interpolation method for $j_0 = 7$ of the 8+66 (R2) reaction (see Fig. 7). From these ICSs, the initial state-specific reaction rate coefficients for $j_0 \le 21$ can be obtained, according to Eq. (1). The reaction rate coefficients for initial states with $j_0 \ge 23$ were approximated by extrapolation described below

$$\ln\left[k_{v_0 j_0}(T)\right] = \frac{E_{j_0^b} - E_{j_0}}{E_{j_0^b} - E_{j_0^a}} \left\{ \ln\left[k_{v_0 j_0^a}(T)\right] - \ln\left[k_{v_0 j_0^b}(T)\right] \right\} + \ln\left[k_{v_0 j_0^b}(T)\right]. \quad (5)$$

In our calculations, j_0^b and j_0^a were set to 21 and 19, respectively. This extrapolation is based on an empirical observation of the initial state-specific rate coefficients, which decrease with increasing j_0 in a predicable way, as discussed in more detail below.

III. RESULTS AND DISCUSSION

A. Numerical parameters

The numerical parameters applied in the calculations are listed in Table I. Since the rate coefficients at relatively low temperatures are mostly controlled by the near-threshold reactivity in these near-thermoneutral reactions, it is vital to accurately determine the ICS at extremely low collision energies, which in a time-dependent wavepacket calculation requires an elaborate treatment of the absorbing potential. We have performed extensive numerical tests to explore this issue. The 8+66 (R2) reaction is slightly exoergic and only a long absorbing potential along the R degree of freedom is required. However, the 6+88 (R1) reaction also requires an absorbing potential in a long grid range for r degree of freedom, because the products may emerge with extremely low kinetic energies.

As can be seen from the results shown in Figs. 1(a) and 1(b) using the DLLJG PES, when the parameters of sets A and B are applied, the total reaction probabilities with $J = 0$ and initial state $j_0 = 1$ exhibit rapid and sharp oscillations below the threshold energy for the endoergic 6+88 (R1) reaction, which are apparently unphysical. On the other hand, there are no such "ghost" oscillations for the exoergic reaction. When the parameters of set C are applied, which adopts a larger grid range and longer-range absorbing potential, the calculations give converged results which agree very closely with those calculated by applying much larger grid parameters. The parameters of sets A, B, and C are listed in Table I. In the calculations below, the results with extremely low collision energies are obtained by using the parameters of set C. However, in calculations with higher collision energies, the parameters of

TABLE I. Numerical parameters for the quantum WP calculations of the $O + O_2$ reactive scattering (all in atomic units, except specified). The three variables of (R, r, θ) define the reactant Jacobi coordinates, where r is the bond distance for the diatomic reactant, R is the distance from the atom to the centre of the mass of the diatomic reactant, and θ is the angle between r and R. $j_{\min}$ and $j_{\max}$ denote the basis size of the Legendre polynomials for θ. For the definition of other parameters, the reader is referred to Ref. 37.

$O + O_2$	Set A	Set B	Set C
Grid/basis range and size	$R \in [0.3, 16.0]$, $N_R^1 = 255$, $N_R^2 = 161$ $r \in [1.5, 7.5]$, $N_r^1 = 99$, $N_r^2 = 31$ $j_{\min} = 0 \sim j_{\max} = 120$, $N_j = 61$	$R \in [0.3, 16.0]$, $N_R^1 = 255$, $N_R^2 = 161$ $r \in [1.5, 14.0]$, $N_r^1 = 161$, $N_r^2 = 31$ $j_{\min} = 0 \sim j_{\max} = 120$, $N_j = 61$	$R \in [0.3, 25.0]$, $N_R^1 = 399$, $N_R^2 = 242$ $r \in [1.5, 25.0]$, $N_r^1 = 319$, $N_r^2 = 47$ $j_{\min} = 0 \sim j_{\max} = 220$, $N_j = 111$
Initial wavepacket $\exp\left[-\frac{(R-R_0)^2}{2\Delta_R^2} + ik_0 R\right]$ with $k_0 = \sqrt{2E_0\mu_R}$	$R_0 = 10.0, \Delta_R = 0.12, E_0 = 0.25eV$	$R_0 = 10.0, \Delta_R = 0.12, E_0 = 0.25eV$	$R_0 = 11.0, \Delta_R = 0.3, E_0 = 0.05eV$
Absorbing potential	$C_a' = 0.001, C_b' = 0.003$, $R_a = 11.0, R_b = 15.0$	$C_a' = 0.001, C_b' = 0.003$, $R_a = 11.0, R_b = 15.0$	$C_a' = 0.0005, C_b' = 0.002, R_a = 13.0, R_b = 23.0$
$n' = n = 1$	$C_a = 0.002, C_b = 0.01$, $r_a = 4.7, r_b = 6.7$	$C_a = 0.003, C_b = 0.02$, $r_a = 9.0, r_b = 13.0$	$C_a = 0.0004, C_b = 0.002, r_a = 12.5, r_b = 23.0$
Propagation	$\Delta t = 120$, total time: 200K a.u.		
Matching plane	...	$R_0' = 7.5$	$R_0' = 11.0$

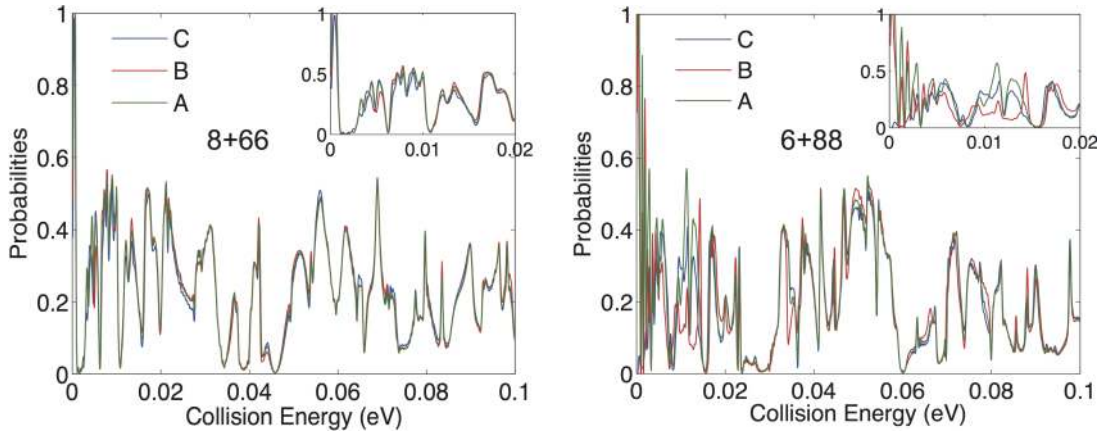

FIG. 1. Total $J = 0$ reaction probabilities for 6+88 (R1) and 8+66 (R2) on the DLLJG PES with parameters of sets A, B, and C, which are listed in Table I.

set A are applied. In this implementation, high accuracy of the numerical results can be achieved with reasonable computational effort.

To highlight the importance of a proper treatment of the threshold effect for the title reactions, we compare the total reaction probabilities with $J = 1$ for initial states of $j_0 = 0$ and 1 in Fig. 2. Immediately above the threshold, there are several reactive resonances which lead to a large peak in the total reaction probabilities for the exoergic 8+66 (R2) reaction, as shown in the left panel. Similar to the energy difference between the $j_0 = 0$ and 1 states, the position of the peak for the latter shifts to a slightly lower collision energy. This results in a considerable difference between the ICSs for these two initial states immediately above the threshold, as shown in Fig. 3 by the top blue and red lines. However, there is not much difference in the ICSs with initial states of $j_0 = 0$ and 1 for the endoergic 6+88 (R1) reaction, as shown by the lower blue and red lines with crosses in Fig. 3. This is due to the negligible difference between the internal energy of $j_0 = 0$ and 1 (about 0.36 meV) compared with the threshold energy (about 2.8 meV), as shown in the right panel of Fig. 2. The ICS for 6+88 (R1) reaction with initial state of $j_0 = 3$ is quite similar to that with $j_0 = 0$ and 1 also, but shifting down to a lower collision energy, as shown by the green line with crosses in Fig. 3. Fig. 3 also shows that it is difficult using the current quantum WP method to accurately calculate the reactive scattering attributes right around (±1 meV) the threshold energy due to the limited propagation time and the limited grid range of the applied absorbing potential.

Due to the different reactivities between the initial states of $j_0 = 0$ and 1 for the 8+66 (R2) reaction, some differences in the initial state-specified reaction rate coefficients for the initial states of $j_0 = 0$ and 1 in the low temperature range for the 8+66 (R2) reaction are expected. Even when the ICSs of these two initial states are quite similar to each other for most collision energies, as shown by the results in Fig. 2, we have to be very careful about the difference between them in the situation where the collision energy is extremely low. This issue was not fully realized in our previous work,[28] although this does not affect the qualitative conclusion on the negative temperature dependence of the rate coefficients. In this work, a much larger grid is used to minimize the error in our calculations.

The ICS of initial state $j_0 = 1$ for the 8+66 (R2) reaction was thus calculated explicitly by using the time-dependent WP method, in contrast to our previous work where the ICS of the initial state $j_0 = 0$ was used to approximate the ICS of initial state $j_0 = 1$.[28] Similarly, due to the threshold effect for the 6+88 (R1) reaction with the initial state as shown in Fig. 3, the ICSs for the initial states of $j_0 = 1$ and 3 were calculated explicitly also. Importantly, the ICSs with collision energy below 8 meV were calculated explicitly using the parameters of set C for

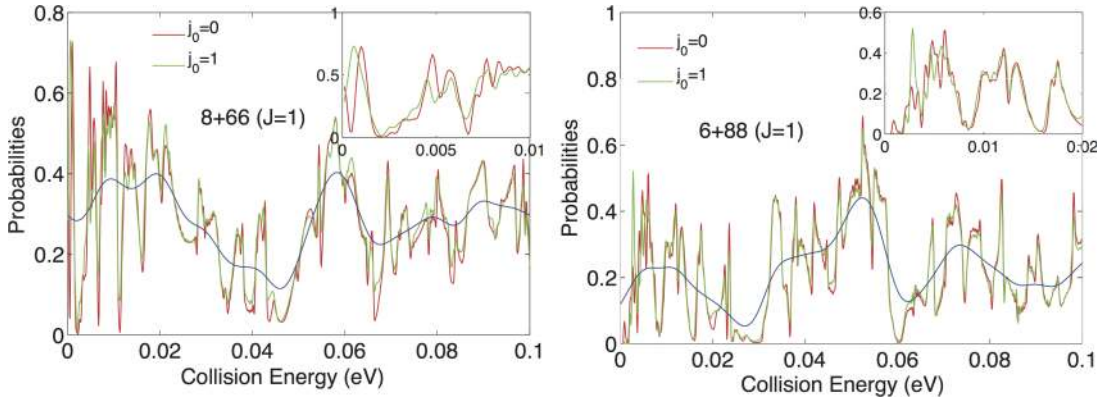

FIG. 2. Comparison of the $J = 1$ total reaction probabilities for 6+88 (R1) and 8+66 (R2) with the initial states of $j_0 = 0$ and 1 on the DLLJG PES. The blue lines are the probabilities with $j_0 = 1$ smoothened by a Gaussian shape function.

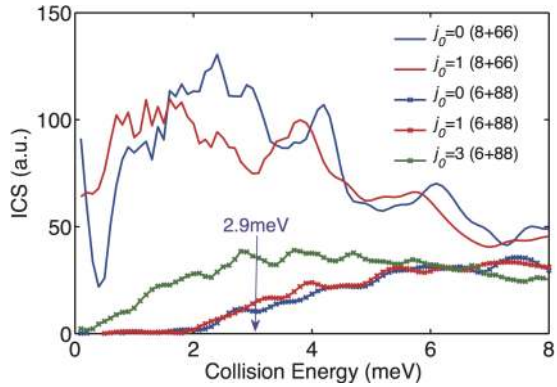

FIG. 3. ICSs for 8+66 (R2) with the initial states of $j_0 = 0$ and 1 and 6+88 (R1) with the initial states of $j_0 = 0$, 1, and 3 at extremely low collision energies using the DLLJG PES. The arrow at 2.9 meV indicates the threshold energy of (R1) with the initial state of $j_0 = 0$.

$J \leq 30$ to guarantee the accuracy of the results just above the threshold.

B. Isotopic effects in the total reaction probabilities

From Fig. 1, it is clear that there are many peaks resulting from dense reactive resonance states, particularly at low collision energies. The situation is similar to what was observed on the mSSB PES in our previous work.[20] To understand the impact of these near-threshold resonances on reactivity, we examine their dependence with both the collision energy and total angular momentum quantum number J, as we did in our previous work.[20] Using a broadening function with a Gaussian shape, which is expressed as

$$f(E_c) = \exp[-\frac{(E_c - E_c^0)^2}{\sigma_E^2}], \quad (6)$$

with σ_E as 0.0041 eV, the oscillations in the total reaction probability for the initial state of $j_0 = 1$ are smoothened (see blue lines in Fig. 2 and also red lines in the upper panels of Fig. 10). The smoothened total reaction probabilities of the reactions (R1) and (R2) are given as a 2D contour plot in Fig. 4. As seen in our previous work on the mSSB PES,[20] the J-shifting rule works well for most collision energy ranges with this reaction, as evidenced by the near quadratic shifts of the peaks with J. This behavior suggests that these so-called "osculating resonances" are controlled by the centrifugal potential imposed by the molecular rotation. The dark purple ridges in the contour plot in the left panel of Fig. 4 indicate that the reaction probabilities of the 8+66 (R2) reaction are larger than those of the 6+88 (R1) reaction (right panel) for most partial waves, due apparently to the stronger resonances in the 8+66 (R2) reaction. As discussed below, this difference translates into the reaction rate coefficients, leading to a large KIE.

C. Isotopic effects in the ICSs and reaction rate coefficients

The total reaction probabilities of the initial rotational states of $j_0 = 1, 5, 9$, and 21 for $J = 0, 10, 30, 50, 70$, and 90 are presented in Fig. 5 for (R1) and (R2), using the DLLJG PES. These data clearly show that the reaction probabilities decrease rapidly for collision energies below 0.2 eV with increasing j_0, due to the disappearance of the resonances.

To understand the decrease of the resonances with increasing j_0 from a stereo-dynamics view point, the total reaction probabilities for $j_0 = 3, 5, 7$, and 9 with different initial K_0 are presented in Fig. 6 with $J = 10$ for the (R1) and (R2) reactions. The plots suggest that the total reaction probabilities for all K_0 values are quite similar and decrease with increasing j_0, except for $K_0 = j_0$ and $j_0 - 1$. It is interesting to observe that for $K_0 = j_0 - 1$, the reaction probabilities are largest for collision energies below 0.2 eV among all K_0 and suggest that it leads to strongest reactive resonances. However, for $K_0 = j_0$, the reaction probabilities are the largest for collision energies above 0.2 eV among all K_0 values. None of the reaction probabilities for $K_0 = j_0$ and $K_0 = j_0 - 1$ are larger than those for $j_0 = 0$ with $J = 10$ in the studied collision energy range. Thus, the total reaction probabilities decrease rapidly with increasing j_0. Similar results were obtained for the (R1) reaction. The decreasing of reactivity with increasing j_0 results from the narrow bottleneck in the angular degree of freedom,[27] which makes the approach less favorable for rotationally excited reactants.

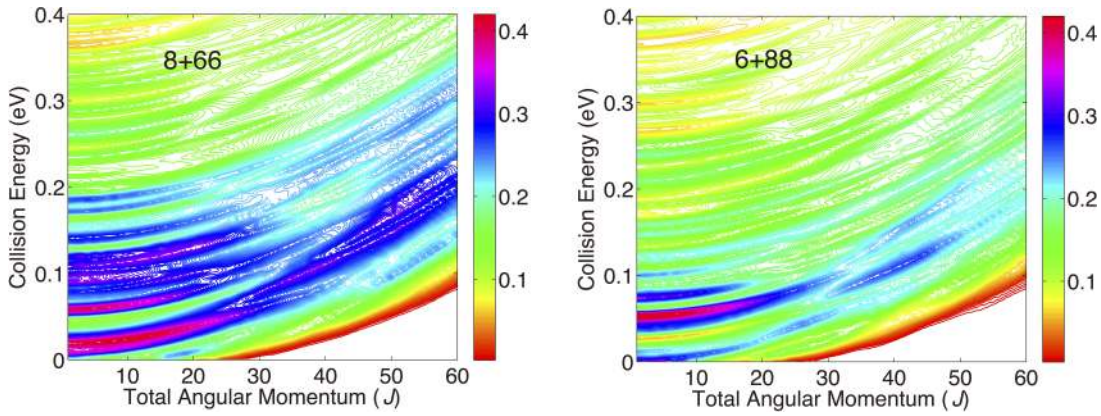

FIG. 4. 2D plot of smoothened total reaction probabilities as a function of collision energy and total angular momentum J for 6+88 (R1) and 8+66 (R2) using the DLLJG PES, with the initial state $j_0 = 1$. The J-shifting rule is clearly observed in both panels, and the reactivity of (R2) is larger for collision energies below 0.2 eV, resulting apparently from the resonance enhancement.

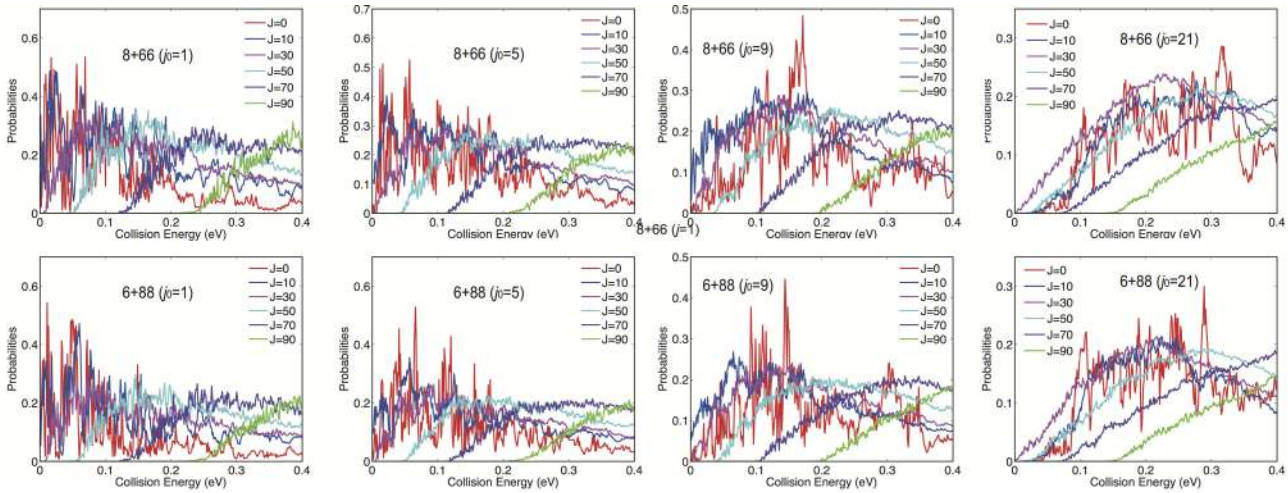

FIG. 5. Total reaction probabilities as a function of collision energy at selected J values for different initial rotational states ($j_0 = 1$, 5, 9, and 21) of 6+88 (R1) and 8+66 (R2) using the DLLJG PES.

Total ICSs for all initial rotational states for both (R1) and (R2) are given in Fig. 7, where the ICSs for j_0 = 1, 3, 5, 9, and 21 have been calculated explicitly using the WP method on the DLLJG PES and for other j_0 the ICSs were estimated using the j_0-interpolation method.

For the 8+66 (R2) reaction, it is clearly seen from Fig. 7 that the ICSs for the initial states of j_0 = 1 and 3 are very similar for most collision energies. And the ICSs for higher initial rotational states become smaller, especially with low collision energies. However, for the 6+88 (R1) reaction, the ICSs for the initial states of j_0 = 1, 3, and 5 at low collision energies are quite different because of its small threshold energy due to the ZPE difference between the diatomic reactant and product, as shown in Fig. 7. The ICSs for the 6+88 (R1) reaction of initial states with j_0 higher than 5 decrease also with increasing j_0, especially at low collision energies, since there is no threshold for these initial states, similar to those of the 8+66 (R2) reaction.

The ICSs with the initial states of j_0 = 1, 3, 5, and 7 for the 8+66 (R2) reaction decrease monotonically with collision energy in the studied collision energy range (except for small oscillations). However, the ICSs with the initial states of higher rotational quantum numbers first decrease and then increase as a function of collision energy. Similar phenomena were observed for the reaction for the 6+88 (R1) reaction with $j_0 \geq 9$. The ICSs with the initial states of j_0 = 1 and 3 for the 6+88 (R1) reaction increase from 0 to a peak value and then decrease with increasing collision energy. Clear humps in the ICSs enhanced by the reactive resonances around the collision energy of 0.06 eV are observed in Fig. 7 for the 6+88 (R1) reaction. The ICSs of the 8+66 (R2) reaction are much larger than the corresponding ones of the (R1) reaction.

To examine the accuracy of the j_0-interpolation method, the ICS with j_0 = 7 of the 8+66 (R2) reaction was calculated explicitly using the quantum WP method. The comparison in Fig. 7 suggests that our j_0-interpolation method is quite accurate.

From the ICSs in Fig. 7, the initial state-specified rate coefficients are calculated and shown in Fig. 8. As we expected from the state-specific ICSs, the reaction rate coefficients for the initial states of lower rotational quantum numbers are larger for both reactions at most temperatures. The rate

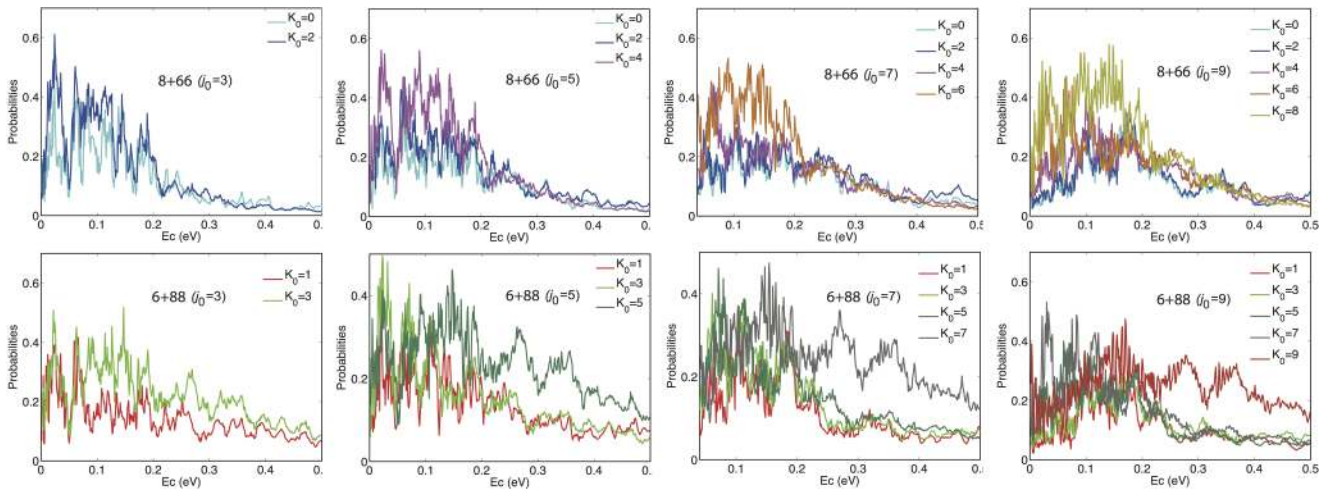

FIG. 6. Total reaction probabilities with different values of (j_0, K_0) for J = 10 of 6+88 (R1) and 8+66 (R2) using the DLLJG PES.

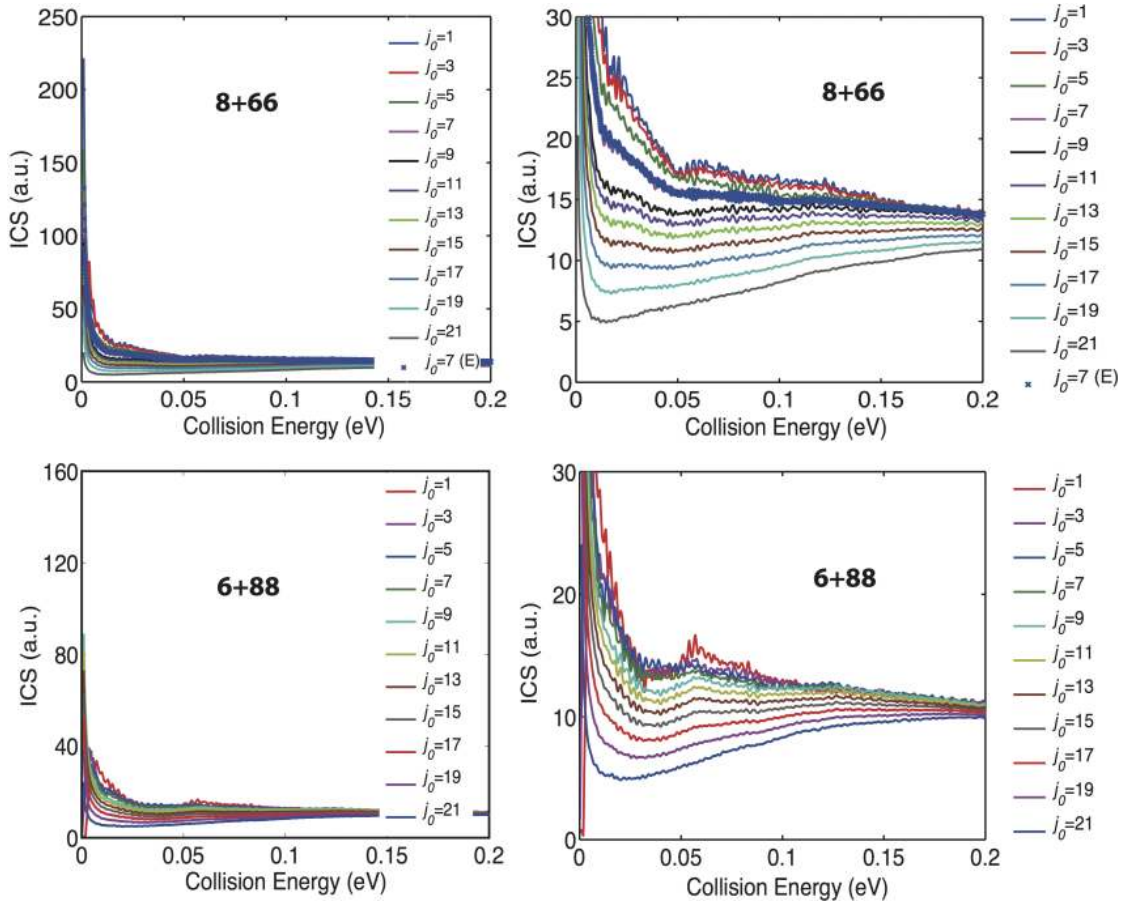

FIG. 7. Initial state-specific ICSs for 6+88 (R1) and 8+66 (R2), calculated on the DLLJG PES by the quantum WP method for $j_0 = 1$, 5, 9, and 21 and by the j-interpolation method for other j_0 values. The ICS of labeled by "$j_0 = 7$ (E)" is explicitly calculated by the quantum WP method for justifying the accuracy of the j-interpolation method.

coefficients with j_0 = 1, 3, and 5 for the 8+66 (R2) reaction exhibit clear negative temperature dependences. However, the negative temperature dependences of the initial state-specified rate coefficients for the 6+88 (R1) reaction are not so obvious. Indeed, those with j_0 = 1 and 3 exhibit clear positive temperature dependences.

The overall thermal reaction rate coefficient can be calculated by Boltzmann averaging all of these state-specific reaction rate coefficients. At a temperature of 400 K, the rotational state populations of the $^{36}O_2$ molecule suggest that initial state-specified rate coefficients of rotational quantum numbers up to 29 have to be included for calculating the thermal reaction rate coefficient by Boltzmann averaging.

The ICSs for initial rotational states with quantum numbers higher than 21 are unavailable by the j_0-interpolation method since the ICSs have only been calculated for initial states with rotational quantum numbers up to 21. However, it is observed in Fig. 8 that there is a predictable variation in the

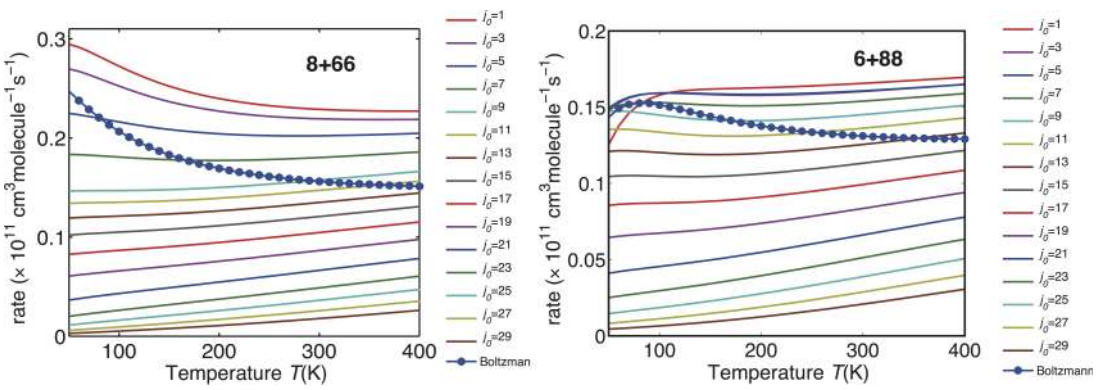

FIG. 8. Initial state-specified reaction rate coefficients as a function of temperature for 6+88 (R1) and 8+66 (R2), calculated from the ICSs given in Fig. 7 and the empirical extrapolation method.

different initial state-specified reaction rate coefficients. With increasing j_0, the reaction rate coefficients decrease monotonically. Thus, the remaining reaction rate coefficients for the initial states with rotational quantum numbers larger than 21 were estimated by extrapolation, as described in Eq. (5). This empirical approach may not be very accurate. However, since the reaction rate coefficients for initial states with rotational quantum numbers larger than 21 contribute relatively little to the thermal reaction rate coefficient in the studied temperature range, this extrapolation likely does not introduce much uncertainty.

The thermal reaction rate coefficients of these two reactions calculated by Boltzmann averaging over all of the state-specific reaction rate coefficients are shown in Fig. 8. Negative temperature dependence of the overall thermal rate coefficients is observed for both reactions, even though many of the initial state-specified reaction rate coefficients do not individually exhibit clear negative temperature dependence.

The initial state-specified reaction rate coefficients (computed by integrating the cross sections over the collision energy, Eq. (1)) include the effect of the electronic partition function factor which varies from a low-temperature limit of 1/15 to a high-temperature limit of 1/27 (Eq. (2)). Thus, the electronic partition function (which assumes statistical population of the asymptotic fine-structure levels and an adiabatic connection of just one of the lowest components to the reactive PES) contributes a factor with significant negative temperature dependence. Despite that, as seen in Fig. 8, only the j_0 = 1, 3, and 5 initial state-specific rate coefficients for 8+66 (R2) (and none of the rate coefficients for (R1)) individually show a clear negative temperature dependence. However, since the initial state-specific rate coefficients drop significantly with j_0, then due to the increasing contributions to the thermal average from higher j_0 with increasing temperature (especially considering the $2j_0 + 1$ degeneracy), the overall rate coefficients take on negative temperature dependences.

To obtain a detailed comparison of the reaction rate coefficients of the (R1) and (R2) reactions, the thermal reaction rate coefficients are presented in the upper panel of Fig. 9. The ratio between the thermal reaction rate coefficient of the (R1) and (R2) reactions is given in the lower panel of Fig. 9. The relevant experimental measurements with 2σ error bars are presented also. The absolute rate coefficients are still somewhat lower than the experimentally derived curves and the calculated negative temperature dependence is not as steep.

The latest DLLJG PES is expected to be more accurate than all other currently available PESs for describing the O + O_2 exchange reaction, yet there are still discrepancies between theory and experiment. There are several possible reasons for the remaining discrepancies. First, accepting the experimental results from Refs. 1–4 (which are all in fairly close agreement), there are a few possibilities on the theoretical side. Considering the PES, while the attractiveness of the long-range should be very accurate (high-level calculations used to fit the PES agree closely and connect smoothly with an asymptotic electrostatic model), it is still possible that the transition region may be even more attractive than what is reflected on the DLLJG PES. The attractiveness in this region (and presence/absence of a reef) as discussed previously,[26,27] even

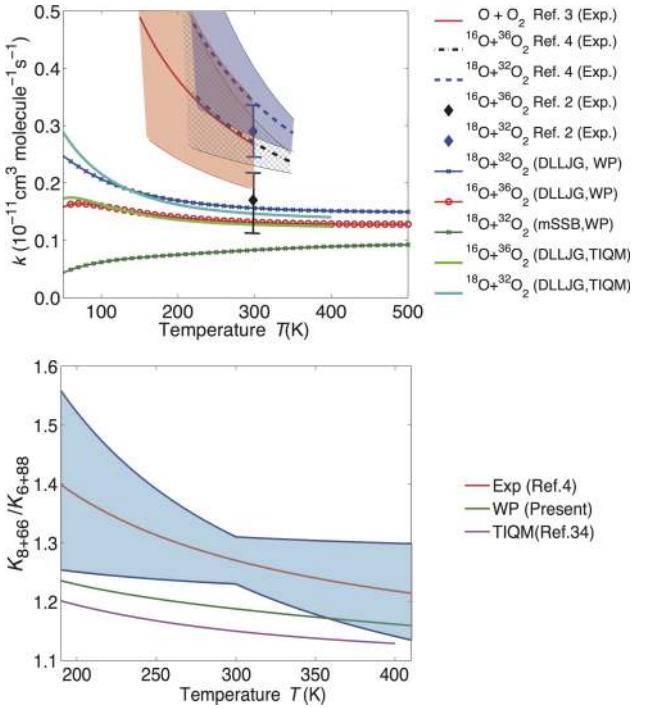

FIG. 9. A comparison of thermal reaction rate coefficients of 6+88 (R1) and 8+66 (R2) calculated using the quantum WP method (upper) and their ratio as a function of temperature (bottom) between the reactions of (R2) and (R1) along with the relevant experimental results. The corresponding TIQM results on the DLLJG PES given in Ref. 34 also are shown for comparison. The boundaries of the shadows indicate the experimental 2σ uncertainty.

with large basis sets (or explicitly correlated F12 methods), is sensitive to high-order electron correlation and the related necessary Davidson correction, as well as internal contraction error. A second possibility is the neglect of non-adiabatic transitions between the 27 fine-structure levels in the asymptotic region. As mentioned above, an adiabatic model was assumed here, in which only the lowest adiabatic state is included in the scattering calculations. We have previously discounted significant contributions from this non-adiabatic effect (confirming the same conclusion by Schinke[44]) based on approximate 2D quantum capture calculations using fitted coupled surfaces for 45 fine-structure levels,[26] but a more rigorous investigation might be warranted. Third, the geometric phase effect could contribute to the dynamics and has been discussed for ozone but has not been treated in quantum dynamics studies of the rate coefficients. This effect is due to the Jahn-Teller distortion that causes ozone to prefer three deep equivalent wells over the higher symmetry D_{3h} configuration. Studies of this effect in cyclic N_3 have predicted dramatic effects on the states and spectroscopy of that system.[45,46] The geometric phase effect is expected to be pronounced in N_3 which has a low barrier to pseudo-rotation. Ozone has a very high barrier to pseudo-rotation and thus the effect should be much smaller than in N_3, but this remains an avenue for further research especially if other possibilities are eliminated.

It is also possible that the discrepancies are due to experimental errors. The three experimental studies described in Refs. 1–4 agree quite closely on the rate coefficients for (R1) and (R2) but are all based on some assumptions on the rate coefficients of O_3 formation and destruction and isotope

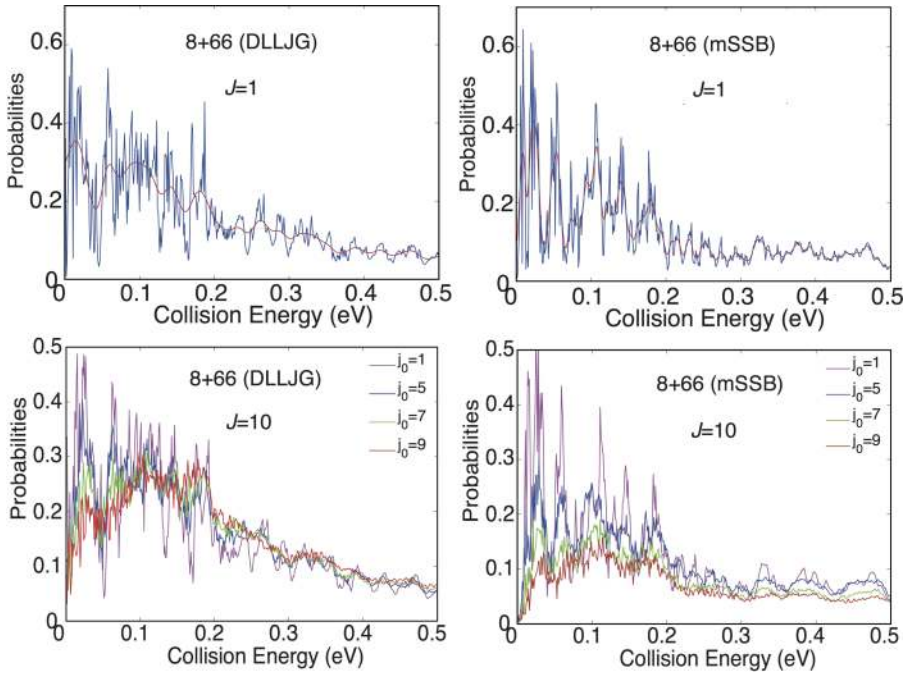

FIG. 10. A comparison of total reaction probabilities for 8+66 (R2) with the initial states of $j_0 = 1$ for $J = 1$ (upper panels) and $j_0 = 1$, 5, 7, and 9 for $J = 10$ (lower panels) using the mSSB and DLLJG PESs. The red lines in the upper panels are the probabilities smoothened by a Gaussian shape function.

dependent UV absorption cross sections. The most recent study is Ref. 4, which treats a temperature range from 233 to 353 K, resulting in large uncertainty in the temperature dependent exponent for the derived rate coefficient. The ^{16}O and ^{18}O atoms were produced by 185 ± 5 nm UV light. Fine-structure branching ratios from photodissociation of oxygen molecules at different wavelengths have been reported to be non-statistical.[47,48] Nevertheless, even the lower 2σ error bar exhibits clear negative temperature dependence with the theoretical result just below.

The theoretical ratio of the rate coefficients for the 8+66 (R2)/6+88 (R1) reactions agrees reasonably with the experimental results, which is much larger than the value estimated from the zero point energy effects. At room temperature, for example, the value of the theoretical ratio is 1.2, as comparing with the experimental ratio of 1.27. This is contrasted with the fact that the ZPE difference is only ±23 cm^{-1} and much smaller than the thermal energy at room temperature ($2k_bT$ = 440 cm^{-1}).

The thermal reaction rate coefficients of (R1) and (R2) and their ratio calculated by a time-independent quantum mechanical (TIQM) method using the hyperspherical coordinates[34] are also shown in Fig. 9. There is a slight difference, mostly within 1%, between the results by the TIQM and our WP methods. Interestingly, the ratio given by our WP method agrees better with the experimental measurements. The smaller values of the WP reaction rate coefficients in the low temperature range of both (R1) and (R2) may be due to the errors in our WP calculations at extremely low collision energies. However, the reason for the slight difference between these two methods in the high temperature range is not clear. It is possibly caused by the approximations applied in this work, such as the J-shifting, j_0-interpolation, and j_0-extrapolation approximations. On the other hand, some numerical uncertainty is likely present in the TIQM method due to a finite basis set and due to the use of a K_{max} approximation with J and j_0 of large values.

D. Comparison of the mSSB and DLLJG PESs

In this section, we will examine the thermal rate coefficients calculated on the mSSB PES using the same protocol described above. Particular attention will be placed on near threshold resonances and the temperature dependence of the thermal rate coefficients.

The $J = 1$ total reaction probabilities with the initial state of $j_0 = 1$ calculated on the mSSB and DLLJG PESs are compared in the upper panels of Fig. 10 as a function of collision energy for the 8+66 (R2) reaction. It is observed that the reactivity on these two PESs is similar, except for the faster decrease of the resonance peaks with increasing collision energy in a more sudden way on the mSSB PES. Due to the "reef" structure, the resonance peaks are sharper on the mSSB PES.

For $J = 10$, the total reaction probabilities of the 8+66 (R2) reaction for the initial states of $j_0 = 1$, 5, 7, and 9 on the mSSB PES are presented in the bottom panels of Fig. 10. It is seen in the figure that the reactivity decreases more rapidly with increasing j_0 than that on the DLLJG PES. In addition, it is also observed that the resonances of the 8+66 (R2) reaction are attenuated much more quickly with increasing J on the mSSB PES than on the DLLJG PES.

Using the same Gaussian broadening function, the smoothened total reaction probabilities of the reactions (R1) and (R2) as a function of collision energy and all J values are given as 2D contour plots in Fig. 11, with the initial state $j_0 = 1$ using the mSSB PES. It is seen that the J-shifting rule works well for most of the collision energy range with this reaction, similar to the results on the DLLJG PES as shown in Fig. 4. Indeed, the purple ridges in the left panel of Fig. 11 indicate that the reaction probabilities of the 8+66 (R2) reaction are somewhat larger than those of the 6+88 (R1) reaction for most partial waves, which suggests that there are stronger resonances and a larger rate coefficient in the 8+66 (R2) reaction on the mSSB

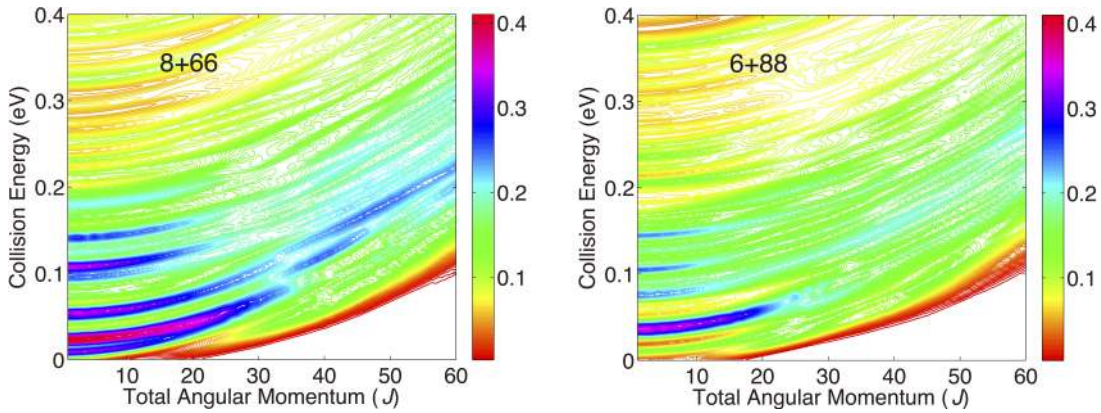

FIG. 11. 2D plot of smoothened total reaction probabilities as a function of collision energy and total angular momentum J of 6+88 (R1) and 8+66 (R2), with the initial state of $j_0 = 1$ on the mSSB PES. The J-shifting rule is clearly observed in both plots, and the reactivity of (R2) is larger at collision energies below 0.15 eV, resulting from the resonance enhancement.

PES also. The purple ridges in Figs. 4 and 11 are indeed quite similar, suggesting the robustness of these quantum resonances in the O + O_2 reaction on these two different PESs.

Since the inclusion of higher rotational states is known to depress the thermal reaction rate coefficient at higher temperatures (see discussion above), the reaction rate coefficients of rotationally excited states of the diatomic reactant need to be calculated to examine the temperature dependence of the thermal reaction rate coefficient on the mSSB PES, which has never been done before. The ICSs of relevant initial states calculated using the time-dependent WP method and j_0-interpolation are shown in the left panel of Fig. 12 for 8+66 (R2). The ICS of $j_0 = 1$ and 3 is nearly identical, and the ICSs of initial states with higher rotational quantum numbers are smaller, especially at collision energies below 0.1 eV. The resonance enhancement to the ICS with initial rotational states of lower quantum numbers at low collision energies is obvious. In contrast, the ICSs of $j_0 = 9$–19 monotonically increase with the collision energy. This is similar to the behavior on the DLLJG PES.

Using the ICS in the left panel of Fig. 12, the initial state-specified rate coefficients for 8+66 (R2) are calculated and shown in the right panel of Fig. 12. As we expected from the state-specific ICSs, the reaction rate coefficients of initial rotational states with lower reactant rotational quantum numbers are larger, similar to those on the DLLJG PES. However, none of them exhibits negative temperature dependence, in contrast with those calculated on the DLLJG PES. The reaction rate coefficients for initial states with $j_0 \geq 21$ are calculated by the j_0-extrapolation approximation, as was done for the (R1) and (R2) reactions on the DLLJG PES. The thermal reaction rate coefficient by Boltzmann averaging overall all of the relevant initial rotational states is shown in Fig. 12 for 8+66 (R2), which does not exhibit negative temperature dependence either. Thus, the removal of the "reef" structure is crucial for reproducing the negative temperature dependence in the reaction rate coefficient. This is the most salient success of the recent DLLJG PES.

E. Near-threshold reactive resonances in the O + O_2 reactions

From total reaction probabilities as a function of collision energy, as shown in Figs. 4–6, it is clear that strong reactive resonances arise when the O atom collides with the slowly rotating O_2 molecule with relatively low translational energies. The resonances are weaker in the 6+88 (R1) reaction than those in the 8+66 (R2) reaction and diminish faster in the (R1) reaction with increasing collision energy. Similar to these on the DLLJG PES, there are stronger resonances for the 8+66 (R2) reaction on the mSSB PES, as shown in Fig. 11. This stronger near-threshold reactive resonances on both PESs lead

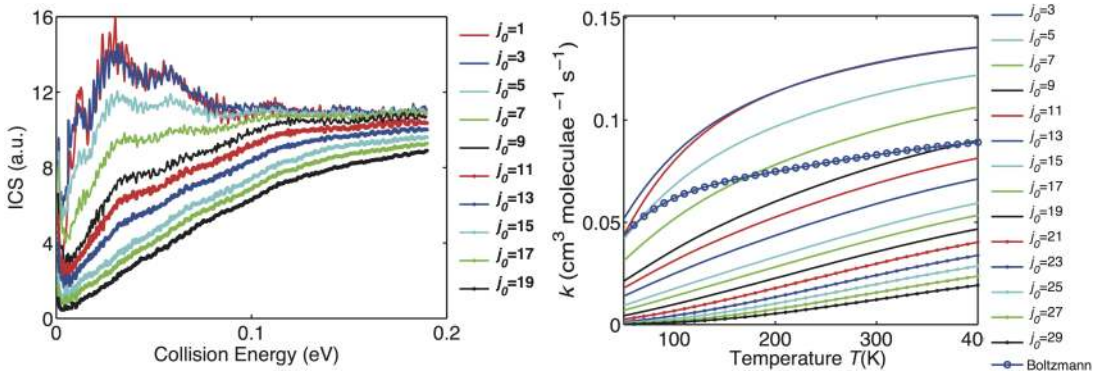

FIG. 12. Initial state-specific ICSs for 8+66 (R2), calculated by the quantum WP method using the mSSB PES (left) and the initial state-specified and thermal reaction rate coefficients (right).

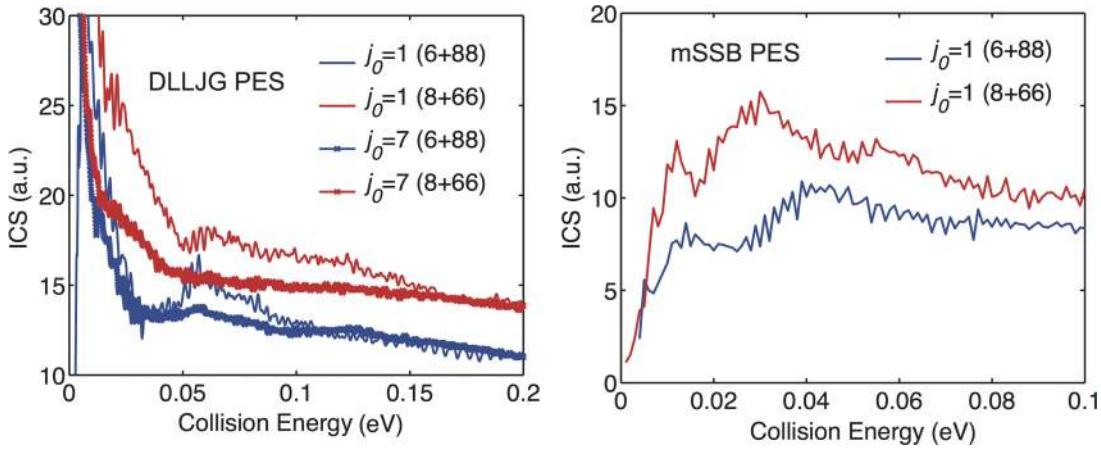

FIG. 13. Initial state-specific ICSs for the 6+88 (R1) and 8+66 (R2) reactions, with the initial states of $j_0 = 1$ and 7 on the DLLJG PES (left) and that for the initial state of $j_0 = 1$ on the mSSB PES. With the same initial state, the ICS of the (R2) reaction is much larger, independent of the PES used in the dynamics calculations.

to larger values of the ICSs and reaction rate coefficients of the 8+66 (R2) reaction, as visualized in Fig. 13.

The presence of the strong resonances in these reactions suggests that breaking of the old bond and formation of a new one are not always a direct process but is facilitated by these metastable states, which are supported by the O_3 PES well and have considerable amplitudes in the asymptotic region of the reactant and product channels. The O_3^* potential well connects to the reactant and product channels via the transition region which is rather narrow in the angular degree of freedom,[24,27] As a result, there is very little chance for the reaction occurring directly. Only the resonances, which are able to effectively break the O–O bond of the short-lived O_3 intermediate, can lead to the occurrence of the reaction. Thus, the resonance states may be regarded as an effective bridge between the reactant and product channels. Due to the lighter masses of the diatomic reactant $^{32}O_2$, there are stronger resonances in the (R2) reaction, which bring about higher reactivity, especially at collision energies below 0.2 eV. Since the mass of the reactant $^{36}O_2$ is larger, the resonances in the (R1) reaction are weaker, which leads to a lower reactivity.

Although the isotopes always lead to differences in ZPE levels in the reactant and product of the exchange reactions, the large KIE in the O + O_2 exchange reaction cannot be attributed to the ZPE difference alone. The mass difference is likely the deeper reason. As shown by the ICSs in Fig. 13 with the initial states of j_0 = 1 and 7, all the ICSs for the 8+66 (R2) reaction are much larger than the corresponding ones for the 6+88 (R1) reaction, independent of the PES used in the calculation. Especially, both the (R1) and (R2) reactions with the initial states of j_0 = 7 are exoergic with an energy release of 44 cm^{-1} and 100 cm^{-1}. The large difference in reactivity in terms of their ICSs cannot thus be explained by direct energy shifting, i.e., the fact that the ICS of 6+88 (R1) shifted to lower collision energy by 56 cm^{-1} does not agree the ICS of 8+66 (R2) for the initial states of j_0 = 7. Anyway, the exact dynamical nature of these near-threshold resonances needs to be explored further with other isotope compositions to ascertain their roles in the KIEs. It is plausible that this resonance induced enhancement effect may explain the symmetry effects in the unusual isotope effects of the O + O_2 reaction,[1] and it would be interesting to compare the resonances and their role in the isotope effects of ozone formation from reactions $^{18}O + {}^{32}O_2 \rightarrow {}^{16}O{}^{16}O{}^{18}O$ and $^{16}O + {}^{16}O{}^{18}O, \rightarrow {}^{16}O{}^{16}O{}^{18}O$ and $^{16}O{}^{18}O{}^{16}O$, as explored in the recent work using a mixed quantum/classical method.[11]

IV. CONCLUSIONS

In this work, we have greatly extended our preliminary WP study on the O + O_2 exchange reaction published in a recent communication,[28] in which the rate coefficient of the $^{18}O + {}^{32}O_2$ reaction was found to be negatively dependent on temperature. In particular, we report here extensive quantum dynamical studies of both the $^{18}O + {}^{32}O_2$ and $^{16}O + {}^{36}O_2$ reactions, using an efficient time-dependent quantum WP method. The ICSs of the $^{18}O + {}^{32}O_2$ and $^{16}O + {}^{36}O_2$ reactions with the initial states of $(v_0, j_0) = (0,1),(0,5),(0,9)$, and (0, 21) have been calculated explicitly on the newly constructed DLLJG PES. The ICSs for other $j_0 \leq 21$ values were estimated by a j_0-interpolation method and those for $j_0 > 21$ were estimated by extrapolation. These ICSs yield the corresponding initial state-specified reaction rate coefficients. Thermal reaction rate coefficients with Boltzmann averaging over all relevant initial states were thus calculated approximately and they exhibit clear negative temperature dependences for both reactions.

Our calculated thermal rate coefficients of the $^{18}O + {}^{32}O_2$ and $^{16}O + {}^{36}O_2$ reactions and the KIE are in good agreement with those reported by Honvault and coworkers using the TIQM method,[34] using the same DLLJG PES. Similar calculations were also carried out on the mSSB PES and the thermal reaction rate coefficients show positive temperature dependence. This provides strong supporting evidence for the accuracy of the DLLJG PES, in which the "reef" structure is absent. We emphasize that an accurate characterization of the reactivity at extremely low collision energies is vital for the accurate determination of the thermal reaction rate coefficients using the DLLJG PES, especially for the endoergic 6+88 (R1) reaction. In such calculations, quantum reactive scattering calculations by a time-dependent WP method require a very large grid.

The total reaction probabilities of the $^{18}O + {}^{32}O_2$ and $^{16}O + {}^{36}O_2$ reactions on the DLLJG PES as a function of the

total angular momentum (J) suggest that the O + O_2 exchange reactions are dominated by resonances at very low collision energies (<0.2 eV) immediately above the reaction threshold. These resonances depend strongly on the masses of the oxygen atoms involved and/or the ZPE difference between the reactant and product diatoms. Though it appears that the isotopic effects in the exchange reactions comes from the ZPE difference, the underlying physical mechanism for the isotope effects is shown here to result from strong near-threshold reactive resonances which mediate the reactions. We believe that this explanation based on these resonance states may be extended to understand the isotopic effects in all of the isotopic exchange reactions, and perhaps also the isotopic effects in the ozone stabilization processes.

The results in this work demonstrate the power and accuracy of the current quantum WP method and the necessity for treating molecular dynamics with quantum principles, even for processes involving atoms with masses as large as that of oxygen atoms.

ACKNOWLEDGMENTS

This work was supported by the National Basic Research Program of China (No. 2013CB922200), the National Natural Science Foundation of China (Grant Nos. 21222308, 21103187, and 21133006), the Chinese Academy of Sciences and the Key Research Program of the Chinese Academy of Sciences, U.S. National Science Foundation (No. CHE-1300945 to R.D.), and U.S. Department of Energy (No. DE-FG02-05ER15694 to H.G.).

[1]S. M. Anderson, F. S. Klein, and F. Kaufman, J. Chem. Phys. **83**, 1648 (1985).
[2]S. M. Anderson, D. Hulsebusch, and K. Mauersberger, J. Chem. Phys. **107**, 5385 (1997).
[3]M. R. Wiegell, N. W. Larsen, T. Pedersen, and H. Egsgaard, Int. J. Chem. Kinet. **29**, 745 (1997).
[4]P. Fleurat-Lessard, S. Y. Grebenshchikov, R. Schinke, C. Janssen, and D. Krankowsky, J. Chem. Phys. **119**, 4700 (2003).
[5]K. Mauersberger, D. Krankowsky, C. Janssen, and R. Schinke, Adv. At., Mol., Opt. Phys. **50**, 1 (2005).
[6]R. Schinke, S. Y. Grebenshchikov, M. V. Ivanov, and P. Fleurat-Lessard, Annu. Rev. Phys. Chem. **57**, 625 (2006).
[7]M. H. Thiemens, Annu. Rev. Earth Planet. Sci. **34**, 217 (2006).
[8]R. A. Marcus, Adv. Quantum Chem. **55**, 5 (2008).
[9]C. Janssen, J. Guenther, K. Mauersberger, and D. Krankowski, Phys. Chem. Chem. Phys. **3**, 4718 (2001).
[10]S. Y. Grebenshchikov and R. Schinke, J. Chem. Phys. **131**, 181103 (2009).
[11]M. V. Ivanov and D. Babikov, Proc. Natl. Acad. Sci. U. S. A. **110**, 17708 (2013).
[12]A. L. Van Wyngarden, K. A. Mar, K. A. Boering, J. J. Lin, Y. T. Lee, S.-Y. Lin, H. Guo, and G. Lendvay, J. Am. Chem. Soc. **129**, 2866 (2007).
[13]A. L. Van Wyngarden, K. A. Mar, J. Quach, A. P. Q. Nguyen, A. A. Wiegel, S.-Y. Lin, G. Lendvay, H. Guo, J. J. Lin, Y. T. Lee, and K. A. Boering, J. Chem. Phys. **141**, 064311 (2014).
[14]Y. Q. Gao and R. A. Marcus, Science **293**, 259 (2001).
[15]R. Siebert, R. Schinke, and M. Bittererova, Phys. Chem. Chem. Phys. **3**, 1795 (2001).
[16]R. Siebert, P. Fleurat-Lessard, R. Schinke, M. Bittererova, and S. C. Farantos, J. Chem. Phys. **116**, 9749 (2002).
[17]D. Babikov, B. K. Kendrick, R. B. Walker, R. T. Pack, P. Fleurat-Lesard, and R. Schinke, J. Chem. Phys. **118**, 6298 (2003).
[18]K.-L. Yeh, D. Xie, D. H. Zhang, S.-Y. Lee, and R. Schinke, J. Phys. Chem. A **107**, 7215 (2003).
[19]S. Y. Lin and H. Guo, J. Phys. Chem. A **110**, 5305 (2006).
[20]Z. Sun, L. Liu, S. Y. Lin, R. Schinke, H. Guo, and D. H. Zhang, Proc. Natl. Acad. Sci. U. S. A. **107**, 555 (2010).
[21]R. Schinke and P. Fleurat-Lessard, J. Chem. Phys. **122**, 094317 (2005).
[22]P. Fleurat-Lessard, S. Y. Grebenshchikov, R. Siebert, R. Schinke, and N. Halberstadt, J. Chem. Phys. **118**, 610 (2003).
[23]R. Hernandez-Lamoneda, M. R. Salazar, and R. T. Pack, Chem. Phys. Lett. **355**, 478 (2002).
[24]R. Schinke and P. Fleurat-Lessard, J. Chem. Phys. **121**, 5789 (2004).
[25]M. Ayouz and D. Babikov, J. Chem. Phys. **138**, 164311 (2013).
[26]R. Dawes, P. Lolur, J. Ma, and H. Guo, J. Chem. Phys. **135**, 081102 (2011).
[27]R. Dawes, P. Lolur, A. Li, B. Jiang, and H. Guo, J. Chem. Phys. **139**, 201103 (2013).
[28]Y. Li, Z. Sun, B. Jiang, D. Xie, R. Dawes, and H. Guo, J. Chem. Phys. **141**, 081102 (2014).
[29]T. R. Rao, G. Guillon, S. Mahapatra, and P. Honvault, J. Phys. Chem. Lett. **6**, 633 (2015).
[30]M. Lepers, B. Bussery-Honvault, and O. Dulieu, J. Chem. Phys. **137**, 234305 (2012).
[31]W. Xie, L. Liu, Z. Sun, H. Guo, and R. Dawes, J. Chem. Phys. **142**, 064308 (2015).
[32]V. G. Tyuterev, R. Kochanov, A. Campargue, S. Kassi, D. Mondelain, A. Barbe, E. Starikova, M. R. De, P. G. Backer, S. Szalay, and Tashkun, Phys. Rev. Lett. **113**, 143002 (2014).
[33]R. Schinke, P. Fleurat-Lessard, and S. Y. Grebenshchikov, Phys. Chem. Chem. Phys. **5**, 1966 (2003).
[34]T. R. Rao, G. Guillon, S. Mahapatra, and P. Honvault, J. Chem. Phys. **142**, 174311 (2015).
[35]W. Li, D. H. Zhang, and Z. Sun, J. Phys. Chem. A **118**, 9801 (2014).
[36]Z. Sun, S.-Y. Lee, H. Guo, and D. H. Zhang, J. Chem. Phys. **130**, 174102 (2009).
[37]Z. Sun, H. Guo, and D. H. Zhang, J. Chem. Phys. **132**, 084112 (2010).
[38]Z. Sun, W. Yang, and D. H. Zhang, Phys. Chem. Chem. Phys. **14**, 1827 (2012).
[39]H. Guo, Int. Rev. Phys. Chem. **31**, 1 (2012).
[40]S. Gómez-Carrasco and O. Roncero, J. Chem. Phys. **125**, 054102 (2006).
[41]D. H. Zhang, S.-Y. Lee, and M. Bear, J. Chem. Phys. **112**, 9802 (2000).
[42]J. M. Bowman, J. Phys. Chem. **95**, 4960 (1991).
[43]A. Gross and G. D. Billing, Chem. Phys. **217**, 1 (1997).
[44]M. Tashiro and R. Schinke, J. Chem. Phys. **119**, 10186 (2003).
[45]D. Babikov, V. A. Mozhayskiy, and A. I. Krylov, J. Chem. Phys. **125**, 084306 (2006).
[46]D. Babikov and B. K. Kendrick, J. Chem. Phys. **133**, 174310 (2010).
[47]Y. Matsumi and M. Kawasaki, J. Chem. Phys. **93**, 2481 (1990).
[48]Y. L. Huang and R. J. Gordon, J. Chem. Phys. **94**, 2640 (1991).